Coordinated Generation Scheduling Considering Peak Regulation Cost Allocation and Compensation Distribution in Power Systems

Yida Yang, Hongjun Gao, Yingmeng Xiang, Minghao Guo, Jiye Wang, and Junyong Liu

***Abstract*—As the share of renewable generations (RGs) in power systems grows, the demand for peak regulation has increased, leading to higher associated costs. In this paper, we propose a mechanism for allocating peak regulation cost among RGs and distributing compensation among peak regulation resources (PRRs). This mechanism is integrated into a coordinated generation scheduling model to enhance the economic efficiency of independent system operators (ISOs) and incentivize PRRs. First, we propose a model for peak regulation cost of diverse PRRs. Next, we develop a method for constructing an RG output curve that facilitates peak regulation. The waveform difference between this constructed curve and the RG forecasted output curve is then calculated. In addition, we create a mechanism for peak regulation cost allocation and compensation distribution that incorporates the waveform difference, the peak regulation contribution of PRRs, and participant satisfaction as key indicators. We then establish a coordinated generation scheduling model using this mechanism, which is solved through the column-and-cut generation algorithm and rolling optimization. Finally, we conduct case studies based on an improved IEEE 30-bus test system and perform several comparative analyses to validate the effectiveness of the proposed mechanism and coordinated generation scheduling model.**

***Index Terms*—Peak regulation cost allocation, renewable generation, compensation distribution, peak regulation resource, coordinated generation scheduling.**

I. Introduction

In recent years, as the penetration rate of renewable energy in power systems has continued to increase, variability and counter peak regulation characteristics [1] of renewable energy outputs have led to a continuous increase in peak-to-valley differences in the net load of power systems [2], thereby increasing peak regulation pressure and costs. Accordingly, designing reasonable mechanisms for the allocation of peak regulation costs and compensation distribution is crucial for building a comprehensive generation-load-storage coordinated generation scheduling method. This is important for enhancing the economic efficiency of independent system operators (ISOs), incentivizing peak regulation resources (PRRs) [3], and improving load supply security and renewable energy consumption [4].

Based on the principle of "causation responsibility", renewable generations (RGs) must be responsible for allocating peak regulation costs, which is typically implemented through the Shapley value and its variants by current research works. Reference [5] proposes a planning-operation model of energy storage system (ESS) for a wind power aggregation station, where the profits of wind farms are distributed to the storage system at the operational level using an improved Shapley method. Reference [6] quantifies the peak regulation costs induced by wind generation integration using the Shapley method to determine the peak regulation costs attributable to each wind turbine (WT). Reference [7] introduces the ratio of deep peak regulation ability and demand as a parameter to improve the short-sight of the original Shapley value allocation method, ultimately proving the efficacy of the modified method through case studies. Some researchers have extended the Shapley value allocation method to other costs. A problem formulation that accounts for the costs of ancillary services, including peak regulation, frequency regulation, and reserves, is proposed in [8], which introduces a model for allocating these costs based on the Shapley value allocation method. However, as the number of renewable generation units increases, the "coalition number" used in the Shapley value allocation method can grow exponentially, making it increasingly challenging to solve the peak regulation cost allocation problem. Clustering algorithms have been adopted by many researchers to extract typical features from numerous resources, thereby achieving dimensionality reduction and rapid analysis. Clustering has been applied in areas such as power forecasting for renewable energy units [9], residential load forecasting [10], and the identification of generation and consumption patterns [11]. Specific clustering methods include the *K*-means and *K*-shape algorithms. In short, clustering methods can be viewed

Manuscript received: July 1, 2024; revised: September 29, 2024; accepted: December 17, 2024. Date of CrossCheck: December 17, 2024. Date of online publication: January 20, 2025.

This work was supported by the National Key R&D Program of China (No. 2022YFB2403400).

Y. Yang, H. Gao, M. Guo (corresponding author), and J. Liu are with the College of Electrical Engineering, Sichuan University, Chengdu, China (e-mail: yyda0529@163.com; gaohongjun@scu.edu.cn; guo_minghao@outlook.com; liujy@scu.edu.cn).

Y. Xiang is with the Department of Electrical and Computer Engineering, Iowa State University, Ames, USA (e-mail: yingmengxiang@gmail.com).

J. Wang is with the China Electric Power Research Institute, Beijing, China (e-mail: wangjiye@epri.sgcc.com.cn).

DOI: 10.35833/MPCE.2024.000705

as a means of striking a balance between computational accuracy and time. However, when applied to peak regulation cost allocation, they may simplify the allocation process, which inevitably reduces the granularity and fairness of the final outcomes, negatively affecting participant enthusiasm. Therefore, it is of urgent need to develop efficient and accurate allocation methods.

Reference [12] assumes that the peak regulation compensation distribution of traditional generation (TG) units is linearly related to the volume of peak regulation. Accordingly, this compensation is incorporated into the objective function of the optimization problem to realize economic scheduling that considers the peak regulation compensation for TG units. However, this method does not sufficiently consider the contribution of peak regulation, making it difficult to encourage the active participation of PRRs. As the types of PRRs in power systems continue to diversify [13], [14], developing more applicable compensation distribution mechanisms for various types of PRRs is imperative.

Reference [15] models the pumped-storage power stations and integrates them with conventional hydropower stations to consider the overall scheduling of a cascaded hydropower plant system as a coordinated generation scheduling between pumped-storage and conventional hydropower stations. Similar to [15], [16] integrates an RC thermal-network-based building aggregation model into the scheduling model of integrated electricity and district heating systems, where the overall scheduling result is considered as the coordinated result. In addition, although some researchers have not considered the result of overall scheduling derived from coordinated generation scheduling, they also have not accounted for the transfer of interests between PRRs under coordinated generation scheduling. Reference [17] proposes a multi-source coordinated peak regulation optimization model that includes nuclear power, conventional power sources, and wind power stations. Although [17] demonstrates good matching characteristics between wind and nuclear power for peak regulation, coordination methods and the transfer of interest in peak regulation between different power sources are not explored. Compared with [17], [18] proposes a scheduling optimization model that considers biogas, solar, and wind energy, utilizing a multi-energy flow coupling matrix to realize coordinated generation scheduling, which considers coordination methods but neglects the transfer of interests. Overall, some coordinated generation-scheduling studies combine the mathematical models of two or more energy resources into a single entity, treating the result of overall scheduling as that of deriving from coordinated generation scheduling. However, this method faces challenges when considering the transfer of interests while fully utilizing the coordinating capabilities of various resources. In addition, as peak regulation pressures and costs continue to increase in future power systems, the economic issues of resources must not be ignored.

In summary, although the coordinated generation scheduling has received considerable attention as a vital measure for maintaining the supply-demand balance, the increasing costs of peak regulation indicate that traditional models that do not consider economic issues of resources have become inadequate. In this paper, we propose a mechanism for peak regulation cost allocation and compensation distribution, based on which we develop a two-stage coordinated generation scheduling model. The main contributions are as follows.

1) The model for peak regulation cost of diverse PRRs is proposed. For a TG unit, the model offers a more refined method than traditional models by accounting for the peak regulation cost incurred from upward ramping. For an ESS, a new coefficient is introduced to represent the increased life-loss cost due to deviation from the regular state of charge (SOC) range, and the life-loss cost from overcharging or overdischarging is considered as the peak regulation cost. For a transferable load (TL), the transfer cost is regarded as the peak regulation cost.

2) A mechanism for peak regulation cost allocation and compensation distribution is proposed. For cost allocation, peak regulation-friendly output curves are introduced as the basis for calculating the allocation ratios for RGs, whereby generation friendliness in cost allocation is considered. The concept of peak regulation contribution is introduced as the basis for compensation distribution. Compared with conventional methods, the proposed mechanism encourages PRRs to participate in peak regulation.

3) Based on the proposed mechanism, a coordinated generation scheduling model is constructed. At the day-ahead phase, the ISO provides pre-scheduling results using the distributionally robust optimization (DRO) framework while simultaneously calculating parameters such as the allocation ratio based on data submitted by the mechanism participants. At the intraday phase, a rescheduling model is established to minimize the ISO subsidy, which is related to participant satisfaction. The coordination process among various resources is reflected in cost allocation and compensation distribution.

The remainder of this paper is structured as follows. In Section II, peak regulation cost modelling (PRCM) is presented. Section III describes the proposed mechanism considering participant satisfaction. Section IV presents a coordinated generation scheduling model considering the proposed mechanism. Section V presents the case study. Section VI concludes the paper.

II. PRCM

A. PRCM for TLs

In practice, because of the large number of nodes in a power system, analyzing and modelling the peak regulation cost at the nodal level is challenging [19], [20]. Therefore, loads in an area can be aggregated into regional loads. Specifically, we assume that the regional load includes a fixed load (FL) and a TL, where TLs participate in incentive-based demand response for peak regulation.

For power system load aggregation, the traditional modularity function is modified using an electrical distance matrix, which serves as the core module of the community detection [21] algorithm to achieve regional segmentation. Following aggregation, the peak regulation cost of TLs can be expressed as [22]:

$$C_{k,t}^{tl,pr}=\left(\Delta P_{k,t}^{tl+}+\Delta P_{k,t}^{tl-}\right)p^{tl} \quad \forall t\in T,\forall k\in N_L \tag{1}$$

where t and T are the index and set of time periods, respectively; k and N_L are the index and set of TLs, respectively; $C_{k,t}^{tl,pr}$ is the TL cost for peak regulation; $\Delta P_{k,t}^{tl+}$ and $\Delta P_{k,t}^{tl-}$ are the transfer-in and transfer-out power of the TL, respectively; and p^{tl} is the unit TL cost.

B. PRCM for TGs

Figure 1 presents the peak regulation process for TGs, where $P_i^{g,b}$ and $P_i^{g,a}$ are the minimum outputs with and without oil-boosting, respectively; $\underline{P}_i^{g,rpr}$ and $\bar{P}_i^{g,rpr}$ are the minimum and maximum outputs in regular peak regulation, respectively; and $\bar{P}_i^{g}$ is the maximum output in upward peak regulation.

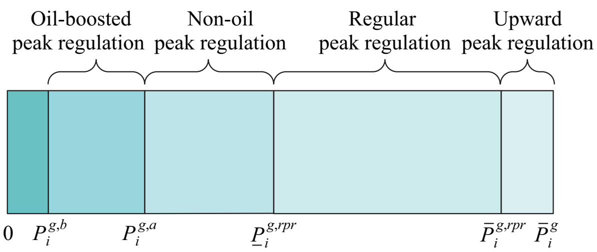

Fig. 1. Peak regulation process for TGs.

1) Modelling for Upward Peak Regulation Cost

At the upward peak regulation stage, the rotor of the generator experiences relatively high temperatures and stresses, which are more likely to lead to rotor creep damage and can result in life-loss costs. The calculation method for the life-loss costs refers to the Manson-Coffin formula [23]. In addition, an excessive load reduces efficiency, necessitating additional fuel consumption. Thus, the upward peak regulation cost of TGs can be expressed as:

$$C_{i,t}^{g,life}=\beta_i\frac{p_i^{g,buy}}{2N_f\left(P_{i,t}^{g}\right)} \quad \forall t\in T,\forall i\in N_G \tag{2}$$

$$\begin{cases} C_{i,t}^{g,adcoal}=\left(\dfrac{P_{i,t}^{g}}{\bar{P}_i^{g,rpr}}-1\right)C_{i,t}^{g,coal} & \forall t\in T,\forall i\in N_G \\ C_{i,t}^{g,coal}=p_i^{g}P_{i,t}^{g} & \forall t\in T,\forall i\in N_G \end{cases} \tag{3}$$

where i and N_G are the index and set of TGs, respectively; $C_{i,t}^{g,coal}$, $C_{i,t}^{g,life}$, and $C_{i,t}^{g,adcoal}$ are the coal cost at regular peak regulation stage, life-loss cost, and additional coal cost at upward peak regulation stage, respectively; $P_{i,t}^{g}$ is the output of TGs; p_i^{g} and $p_i^{g,buy}$ are the unit output cost and purchase cost of TGs, respectively; and $N_f(\cdot)$ and β_i are the rotor crack cycle count and loss coefficient, respectively.

2) Modelling for Deep Peak Regulation Cost

At the non-oil peak regulation stage, the output of TG deviates significantly from the design values, leading to a low-cycle fatigue loss of the rotor, which can also be calculated using (2).

At the oil-boosted peak regulation stage, the peak regulation cost includes life-loss, oil, and polluting gas emission costs.

$$C_{i,t}^{g,oil}=Q_i^{g,oil}p^{oil} \quad \forall t\in T,\forall i\in N_G \tag{4}$$

$$C_{i,t}^{g,emi}=p^{SO_2}w_i^{g,SO_2}\left(P_i^{g,a}-P_{i,t}^{g}\right)+p^{NO_x}w_i^{g,NO_x}\left(P_i^{g,a}-P_{i,t}^{g}\right) \quad \forall t\in T,\forall i\in N_G \tag{5}$$

where $C_{i,t}^{g,oil}$ and $C_{i,t}^{g,emi}$ are the oil cost and polluting gas emission cost of TGs, respectively; p^{oil} is the unit oil price; p^{SO_2} and p^{NO_x} are the unit emission costs of SO_2 and NO_x, respectively; $Q^{g,oil}$ is the single oil injection amount; and w_i^{g,SO_2} and w_i^{g,NO_x} are the polluting gas emissions of SO_2 and NO_x caused by a unit output that is lower than $P_i^{g,a}$, respectively.

Overall, the peak regulation cost of TG $C_{i,t}^{g,pr}$ can be expressed as:

$$C_{i,t}^{g,pr}=\begin{cases} C_{i,t}^{g,life}+C_{i,t}^{g,adcoal} & P_i^{g}\in\left(\bar{P}_i^{g,rpr},\bar{P}_i^{g}\right],\forall t,\forall i \\ C_{i,t}^{g,life} & P_i^{g}\in\left[P_i^{g,a},\underline{P}_i^{g,rpr}\right],\forall t,\forall i \\ C_{i,t}^{g,life}+C_{i,t}^{g,oil}+C_{i,t}^{g,emi} & P_i^{g}\in\left[P_i^{g,b},P_i^{g,a}\right),\forall t,\forall i \end{cases} \tag{6}$$

C. PRCM for ESSs

In this paper, the life-loss cost resulting from overcharging or overdischarging of the ESS is considered as the peak regulation cost, which can be expressed as:

$$C_{j,t}^{ess,pr}=\frac{\Delta S_{j,t}^{pr}p_j^{ess,buy}}{2N_j^{cyc}}\lambda_{j,t}^{ess} \quad \forall t\in T,\forall j\in N_{ESS} \tag{7a}$$

$$\Delta S_{j,t}^{pr}=\begin{cases} \left|S_{j,t}^{ess}-S_{j,t-1}^{ess}\right| & \forall S_{j,t}^{ess},S_{j,t-1}^{ess}\notin\left[\underline{S}_j^{ess,rpr},\bar{S}_j^{ess,rpr}\right] \\ S_{j,t}^{ess}-\bar{S}_j^{ess,rpr} & S_{j,t}^{ess}\geq\bar{S}_j^{ess,rpr}\cap S_{j,t-1}^{ess}\in\left[\underline{S}_j^{ess,rpr},\bar{S}_j^{ess,rpr}\right] \\ \underline{S}_j^{ess,rpr}-S_{j,t}^{ess} & S_{j,t}^{ess}\leq\underline{S}_j^{ess,rpr}\cap S_{j,t-1}^{ess}\in\left[\underline{S}_j^{ess,rpr},\bar{S}_j^{ess,rpr}\right] \end{cases} \tag{7b}$$

$$\lambda_{j,t}^{ess}=\begin{cases} \dfrac{S_{j,t}^{ess}}{\bar{S}_j^{ess,rpr}}-1 & \forall S_{j,t}^{ess}\in\left(\bar{S}_j^{ess,rpr},\bar{S}_j^{ess}\right],\forall t\in T,\forall j\in N_{ESS} \\ 0 & \forall S_{j,t}^{ess}\in\left[\underline{S}_j^{ess,rpr},\bar{S}_j^{ess,rpr}\right],\forall t\in T,\forall j\in N_{ESS} \\ \dfrac{\underline{S}_j^{ess,rpr}}{S_{j,t}^{ess}}-1 & \forall S_{j,t}^{ess}\in\left[\underline{S}_j^{ess},\underline{S}_j^{ess,rpr}\right),\forall t\in T,\forall j\in N_{ESS} \end{cases} \tag{7c}$$

where j and N_{ESS} are the index and set of ESSs, respectively; $C_{j,t}^{ess,pr}$ is the peak regulation cost of ESSs; $S_{j,t}^{ess}$ is the SOC of ESSs; $\bar{S}_j^{ess,rpr}$ and $\underline{S}_j^{ess,rpr}$ are the maximum and minimum SOCs of ESSs at regular peak regulation stage, respectively; $\bar{S}_j^{ess}$ and $\underline{S}_j^{ess}$ are the maximum and minimum SOCs of ESSs, respectively; $\Delta S_{j,t}^{pr}$ is the SOC change due to peak regulation; $p_j^{ess,buy}$ is the purchase cost of ESSs; N_j^{cyc} is the number of fully charging and discharging cycles; and $\lambda_{j,t}^{ess}$ is the increase in the life-loss ratio resulting from a deviation from the regular SOC range.

III. Proposed Mechanism Considering Participant Satisfaction

A. Satisfaction Modelling for Mechanism Participants

1) Satisfaction Modelling of RGs

In this paper, RGs include WTs and photovoltaic (PV) systems, which are abbreviated as w and v in subsequent equations. For RGs, if weather conditions change, the actual outputs during certain periods may be significantly lower than the forecasted outputs. In these cases, the power generation income is low, but the demand for upward peak regulation of the system is high, which can result in an undesirable consequence whereby the RGs bear a high ratio of the peak regulation cost related to their income. In these situations, the ISO provides a subsidy, denoted as $C_t^{x,sub}$, to meet the satisfaction constraints of the RGs.

$$\varepsilon_t^x \geq \underline{\varepsilon}^{RG} \quad \forall t \in T, x \in \{w, v\} \tag{8a}$$

$$\varepsilon_t^x = 1 - \frac{C_t^{x,alloc}}{p^e\left(P_t^x - P_t^{x,cur}\right) + C_t^{x,sub}} \quad \forall t, x \in \{w, v\} \tag{8b}$$

where ε_t^x is the participant satisfaction; $\underline{\varepsilon}^{RG}$ is the minimum satisfaction value of RGs; p^e is unit electricity price; P_t^x and $P_t^{x,cur}$ are the forecasted output power and curtailment power of x, respectively; and $C_t^{x,alloc}$ and $C_t^{x,sub}$ are the peak regulation cost allocation for x and the peak regulation subsidy for x, respectively.

2) Satisfaction Modelling of PRRs

PRRs include TGs, ESSs and TLs, which are abbreviated as g, ess, and tl in the subsequent equations. For PRRs, if the peak regulation compensation $C_t^{x,comp}$ is significantly lower than the peak regulation cost $C_t^{x,pr}$, the participant incentive will be reduced in peak regulation. The ISO also provides a subsidy $C_t^{x,sub}$ to meet the satisfaction constraints for the PRRs as shown in (9).

$$\varepsilon_t^x \geq \underline{\varepsilon}^{PRR} \quad \forall t \in T, x \in \{g, ess, tl\} \tag{9a}$$

$$\varepsilon_t^x = 1 - \frac{C_t^{x,pr}}{C_t^{x,comp} + C_t^{x,sub}} \quad \forall t \in T, x \in \{g, ess, tl\} \tag{9b}$$

where $\underline{\varepsilon}^{PRR}$ is the minimum satisfaction value of PRRs.

B. Cost Allocation Based on Peak Regulation-friendly Output Curves

1) Construction of Peak Regulation-friendly Output Curves

Based on a directrix-based demand response [24], we define the peak regulation-friendly output curves of RGs as the output curves obtained by adjusting the forecasted output curves under certain constraints. When the RGs generate power according to the peak regulation-friendly output curves, the peak regulation demand in the power system will be minimized, in this case, the RGs can be regarded as friendly to the power system.

We consider the construction of peak regulation-friendly output curves as an optimization problem, which aims to minimize the peak regulation demand. The total power generation invariance, adjustment threshold, and peak-valley characteristics serve as the main constraints. The objective function is expressed as:

$$\min f = a^g f^g + a^{ess} f^{ess} + a^{tl} f^{tl} \tag{10a}$$

$$f^g = \frac{1}{T}\sum_{i \in N_G, t \in T}\left(P_{i,t}^g - P_i^{g,avg}\right)^2 \tag{10b}$$

$$f^{ess} = \frac{1}{T}\sum_{j \in N_{ESS}, t \in T}\left(S_{j,t}^{ess} - S_j^{ess,avg}\right)^2 \tag{10c}$$

$$f^{tl} = \sum_{k \in N_L, t \in T}\left(\Delta P_{k,t}^{tl+} + \Delta P_{k,t}^{tl-}\right) \tag{10d}$$

where a^g, a^{ess}, and a^{tl} are the normalization coefficients; f^g, f^{ess}, and f^{tl} are the objective functions for TGs, ESSs, and TLs, respectively; and the superscript avg denotes the average value. Equation (10a) represents the weighted minimum of the variance of RG time-sequenced outputs, the variance of the ESS time-sequenced SOC, and the transfer power of the TLs.

The primary constraints can be expressed as:

$$\begin{cases} \sum_{t \in T} P_t^{x,fri} = \sum_{t \in T} P_t^x & x \in \{w, v\} \\ \dfrac{\left|P_t^{x,fri} - P_t^x\right|}{P_t^x} \leq v_x & \forall t \in T, x \in \{w, v\} \\ P_{t_1}^{x,fri} \leq P_{t_2}^{x,fri} & \forall t_1 \in T_{tr}^x, \forall t_2 \in T_{pk}^x, x \in \{w, v\} \end{cases} \tag{11}$$

where v_x is the adjustment threshold; $P_t^{x,fri}$ and P_t^x are the peak regulation-friendly output curve and forecasted output curve of x, respectively; and T_{pk}^x and T_{tr}^x are the sets of peak periods and valley periods, respectively. Other constraints such as the operation constraints of various resources are similar to those of general economic scheduling. Equation (11) ensures that peak regulation-friendly output curves are objectively reasonable. The curve constructed for each RG serves as the basis for the subsequent calculation of the allocation ratio of peak regulation costs.

2) Calculation of Allocation Ratio Considering Waveform Differences

We use the dynamic time warping (DTW) distance [25] to assess the waveform differences between the normalized forecasted outputs and the peak regulation-friendly output curves. Here, $\widetilde{(\cdot)}$ represents a normalized curve. We assume that the DTW distance between $\tilde{P}_t^{x,fri}$ and $\tilde{P}_t^x$ is $D^x(T,T)$. In addition, the waveform difference ς_t^x during period t is:

$$\varsigma_t^x = \frac{\left|\tilde{P}_t^x - \tilde{P}_t^{x,fri}\right|}{\sum_{t \in T}\left|\tilde{P}_t^x - \tilde{P}_t^{x,fri}\right|} D^x(T,T) \quad \forall t \in T, x \in \{w, v\} \tag{12}$$

$D^x(T,T)$ is subdivided into periods by (12), indicating that the output deviation during each period and the overall friendliness of the outputs during cost allocation are considered.

When determining the allocation ratio of the peak regulation costs, we must also consider the proportion of forecasted power for each RG. The higher the forecasted proportion, the higher the allocation ratio. The allocation ratio during period t is:

$$\varphi_t^x = \frac{P_t^x \varsigma_t^x}{\sum_{x \in \{w,v\}} P_t^x \varsigma_t^x} \quad \forall t \in T, x \in \{w, v\} \tag{13}$$

where φ_t^x is the ratio of peak regulation cost allocation. The total peak regulation cost C_t^{pr} during period t and the amount of peak regulation cost allocation are given as:

$$C_t^{pr} = \sum_{i \in N_G} C_{i,t}^{g,pr} + \sum_{j \in N_{ESS}} C_{j,t}^{ess,pr} + \sum_{k \in N_L} C_{k,t}^{tl,pr} \quad \forall t \in T \tag{14}$$

$$C_t^{x,alloc} = \varphi_t^x C_t^{pr} \quad \forall t \in T, x \in \{w, v\} \tag{15}$$

C. Compensation Distribution Based on Peak Regulation Contribution

We represent the contribution of each PRR by the proportion of each PRR peak regulation power with respect to the total peak regulation power. The peak regulation power is calculated as:

$$P_{i,t}^{g,pr} = \begin{cases} P_{i,t}^{g} - \overline{P}_i^{g,rpr} & P_{i,t}^{g} \geq \overline{P}_i^{g,rpr} \\ \underline{P}_i^{g,rpr} - P_{i,t}^{g} & P_{i,t}^{g} < \underline{P}_i^{g,rpr} \end{cases} \tag{16}$$

$$P_{j,t}^{ess,pr} = \Delta S_{j,t}^{pr} Q_j^{ess} \tag{17}$$

$$P_{k,t}^{tl,pr} = \Delta P_{k,t}^{tl+} + \Delta P_{k,t}^{tl-} \tag{18}$$

where $P_{i,t}^{g,pr}$, $P_{j,t}^{ess,pr}$, and $P_{k,t}^{tl,pr}$ are the peak regulation power of the TGs, ESSs, and TLs, respectively; and Q_j^{ess} is the ESS capacity.

By combining (16)-(18), the total peak regulation power P_t^{pr} during period t and the contribution of each PRR r_t^x are:

$$P_t^{pr} = \sum_{i \in N_G} P_{i,t}^{g,pr} + \sum_{j \in N_{ESS}} P_{j,t}^{ess,pr} + \sum_{k \in N_L} P_{k,t}^{tl,pr} \quad \forall t \in T \tag{19}$$

$$r_t^x = \frac{P_t^{x,pr}}{P_t^{pr}} \quad \forall t \in T, x \in \{g, ess, tl\} \tag{20}$$

Based on the peak regulation contribution, the compensation received by each PRR during period t is:

$$C_t^{x,comp} = r_t^x C_t^{pr} \quad \forall t \in T, x \in \{g, ess, tl\} \tag{21}$$

D. Implementation Method of Proposed Mechanism

Figure 2 shows the implementation method of the proposed mechanism at two stages. At the day-ahead stage, the PRRs and RGs report their parameters, including forecasted electricity load and forecasted output P_t^x, to the ISO. The ISO constructs $P_t^{x,fri}$ based on P_t^x and the PRR parameters. ς_t^x and φ_t^x are also calculated.

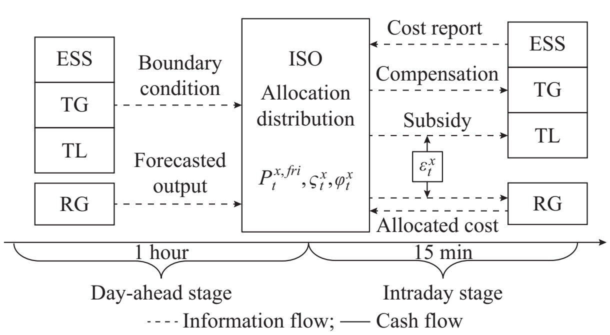

Fig. 2. Implementation method of proposed mechanism.

At the intraday stage, each PRR reports its peak regulation cost to the ISO. The ISO calculates C_t^{pr} and notifies the RGs to pay $C_t^{x,alloc}$ based on φ_t^x. After the RGs pay $C_t^{x,alloc}$, the ISO distributes $C_t^{x,comp}$ to the PRRs based on r_t^x. The ISO also distributes subsidy $C_t^{x,bus}$ to the RGs and PRRs to meet the satisfaction constraints, thus completing the entire cost allocation and compensation distribution.

IV. Coordinated Generation Scheduling Model Considering Proposed Mechanism

A. Day-ahead DRO Pre-scheduling Model

1) Objective Function

The objective function of the day-ahead DRO pre-scheduling model aims to achieve the economic optimum of system operation, which is expressed as:

$$\begin{cases} F_1 = \min\limits_{\boldsymbol{x}} \sum\limits_{t \in T} \sum\limits_{i \in N_G} \left(C_{i,t}^{g,on} + C_{i,t}^{g,off} \right) + \\ \quad \max\limits_{p_s \in \Omega} \min\limits_{\boldsymbol{y}} \mathbb{E}_{\mathrm{p}} \sum\limits_{t \in T} \sum\limits_{i \in N_G} \left(C_{i,t}^{g,coal} + \sum\limits_{j \in N_{ESS}} C_{j,t}^{ess} + \right. \\ \quad \left. \sum\limits_{k \in N_L} C_{k,t}^{l,shed} + \sum\limits_{m \in N_W} C_{m,t}^{w,cur} + \sum\limits_{n \in N_V} C_{n,t}^{v,cur} + C_t^{pr} \right) \\ \boldsymbol{x} = \left[u_{i,t}^{g}, u_{j,t}^{ess,dis}, u_{j,t}^{ess,ch} u_{k,t}^{tl+}, u_{k,t}^{tl-} \right]^{\mathrm{T}} \\ \boldsymbol{y} = \left[P_{i,t}^{g}, P_{j,t}^{ess,ch}, P_{j,t}^{ess,dis}, P_{n,t}^{v,cur}, P_{m,t}^{w,cur}, P_{k,t}^{l,shed} \right]^{\mathrm{T}} \end{cases} \tag{22a}$$

$$C_{i,t}^{g,coal} = P_{i,t}^{g} p_i^{g} \quad \forall t \in T, \forall i \in N_G \tag{22b}$$

$$C_{j,t}^{ess} = \left(\eta_j^{ess,ch} P_{j,t}^{ess,ch} + \frac{P_{j,t}^{ess,dis}}{\eta_j^{ess,dis}} \right) p_j^{ess} \quad \forall t, \forall j \in N_{ESS} \tag{22c}$$

$$C_{n,t}^{v,cur} = P_{n,t}^{v,cur} p^{v,cur} \quad \forall t \in T, \forall n \in N_V \tag{22d}$$

$$C_{m,t}^{w,cur} = P_{m,t}^{w,cur} p^{w,cur} \quad \forall t \in T, \forall m \in N_W \tag{22e}$$

$$C_{k,t}^{l,shed} = P_{k,t}^{l,shed} p^{l,shed} \quad \forall t \in T, \forall k \in N_L \tag{22f}$$

where p_s and Ω are the probability of typical scenario s and the set of confidence distribution of RG output probabilities, respectively; $C_{i,t}^{g,on}$ and $C_{i,t}^{g,off}$ are the start-up and shut-down costs of TGs, respectively; $C_{k,t}^{l,shed}$, $C_{m,t}^{w,cur}$, and $C_{n,t}^{v,cur}$ are the costs of load shedding, WT power curtailment, and PV power curtailment, respectively; $C_{j,t}^{ess}$ is the conventional operation cost of ESSs; $P_{j,t}^{ess,dis}$ and $P_{j,t}^{ess,ch}$ are the charging and discharging power of ESSs, respectively; $P_{k,t}^{l,shed}$ is the load shedding power; $\eta_j^{ess,ch}$ and $\eta_j^{ess,dis}$ are the charging and discharging efficiencies of ESSs, respectively; $\boldsymbol{x}$ and $\boldsymbol{y}$ are the vectors of day-ahead and intraday optimization variables, respectively; $p^{l,shed}$, $p^{w,cur}$, and $p^{v,cur}$ are the unit costs of load shedding, WT power curtailment, and PV power curtailment, respectively; p_j^{ess} is the unit output cost of ESSs; $\mathbb{E}_{\mathrm{p}}$ denotes the mathematical expectation; n and N_V are the set and index of PVs, respectively; and m and N_W are the set and index of WTs, respectively.

2) Constraints

1) Power system balance constraint

$$\sum_{i \in N_G} P_{i,t}^{g} + \sum_{j \in N_{ESS}} \left(P_{j,t}^{ess,dis} - P_{j,t}^{ess,ch} \right) + \sum_{n \in N_V} \left(P_{n,t}^{v} - P_{n,t}^{v,cur} \right) + \sum_{m \in N_W} \left(P_{m,t}^{w} - P_{m,t}^{w,cur} \right) = \sum_{k \in N_L} \left(P_{k,t}^{fl} + P_{k,t}^{tl} - \Delta P_{k,t}^{tl-} + \Delta P_{k,t}^{tl+} - P_{k,t}^{l,shed} \right) \tag{23}$$

where $P_{k,t}^{fl}$ is the load demand of the FLs; and $P_{k,t}^{tl}$ is the load demand of the TLs without considering the transfer.

2) Operation constraints for TGs

$$u_{i,t}^{g} P_{i,t}^{g,b} \le P_{i,t}^{g} \le u_{i,t}^{g} \bar{P}_{i}^{g} \quad \forall i \in N_G, \forall t \in T \tag{24a}$$

$$-R_i^{g,dn} \le P_{i,t}^{g} - P_{i,t-1}^{g} \le R_i^{g,up} \quad \forall i \in N_G, \forall t \in T \tag{24b}$$

$$\sum_{t \in T}^{t+t_i^{g,off}-1} \left(1-u_{i,t}^{g}\right) \le t_i^{g,off}\left(u_{i,t-1}^{g} - u_{i,t}^{g}\right) \quad \forall i \in N_G \tag{24c}$$

$$\sum_{t \in T}^{t+t_i^{g,on}-1} u_{i,t}^{g} \le t_i^{g,on}\left(u_{i,t}^{g} - u_{i,t-1}^{g}\right) \quad \forall i \in N_G \tag{24d}$$

where $R_i^{g,up}$ and $R_i^{g,dn}$ are the ramp-up and ramp-down rates of the TGs, respectively; $t_i^{g,on}$ and $t_i^{g,off}$ are the minimum start-up and shut-down time of the TGs, respectively; and $u_{i,t}^{g}$ is the operation status variable of the TGs.

3) Operation constraints for ESSs

$$u_{j,t}^{ess,dis} + u_{j,t}^{ess,ch} = 1 \quad \forall j \in N_{ESS}, \forall t \in T \tag{25a}$$

$$0 \le P_{j,t}^{ess,dis} \le \bar{P}_{j,t}^{ess,dis} u_{j,t}^{ess,dis} \quad \forall j \in N_{ESS}, \forall t \in T \tag{25b}$$

$$0 \le P_{j,t}^{ess,ch} \le \bar{P}_{j,t}^{ess,ch} u_{j,t}^{ess,ch} \quad \forall j \in N_{ESS}, \forall t \in T \tag{25c}$$

$$\underline{S}_{j}^{ess} \le S_{j,t}^{ess} \le \bar{S}_{j}^{ess} \quad \forall j \in N_{ESS}, \forall t \in T \tag{25d}$$

$$S_{j,t}^{ess} = S_{j,t-1}^{ess} + \eta_j^{ess,ch} \frac{P_{j,t}^{ess,ch}}{Q_j^{ess}} - \frac{P_{j,t}^{ess,dis}}{\eta_j^{ess,dis} Q_j^{ess}} \quad \forall j \in N_{ESS}, \forall t \tag{25e}$$

where $u_{j,t}^{ess,dis}$ and $u_{j,t}^{ess,ch}$ are the discharging and charging statuses of the ESSs, respectively.

4) Operation constraints for TLs

$$u_{k,t}^{tl+} + u_{k,t}^{tl-} = 0 \quad \forall t \in T_{non\text{-}transf} \tag{26a}$$

$$u_{k,t}^{tl+} + u_{k,t}^{tl-} \le 1 \quad \forall t \in T_{transf} \tag{26b}$$

$$0 \le \Delta P_{k,t}^{tl+} \le \upsilon^{tl+} u_{k,t}^{tl+} P_{k,t}^{tl} \quad \forall k \in N_L, \forall t \in T \tag{26c}$$

$$0 \le \Delta P_{k,t}^{tl-} \le \upsilon^{tl-} u_{k,t}^{tl-} P_{k,t}^{tl} \quad \forall k \in N_L, \forall t \in T \tag{26d}$$

$$\sum_{t \in T} \Delta P_{k,t}^{tl-} = \sum_{t \in T} \Delta P_{k,t}^{tl+} \quad \forall k \in N_L \tag{26e}$$

where $T_{non\text{-}transf}$ and T_{transf} are the non-transferable and transferable periods, respectively; $u_{k,t}^{tl+}$ and $u_{k,t}^{tl-}$ are the transfer-in and transfer-out statuses of TLs, respectively; and υ^{tl+} and υ^{tl-} are the maximum transfer-in and transfer-out ratios, respectively.

5) Constraints for power curtailment

$$0 \le P_{n,t}^{v,cur} \le \bar{P}_{n,t}^{v,cur} \quad \forall n \in N_V, \forall t \in T \tag{27a}$$

$$0 \le P_{m,t}^{w,cur} \le \bar{P}_{m,t}^{w,cur} \quad \forall m \in N_W, \forall t \in T \tag{27b}$$

6) Constraint for load shedding

$$0 \le P_{k,t}^{l,shed} \le \bar{P}_{k,t}^{l,shed} \quad \forall k \in N_L, \forall t \in T \tag{28}$$

7) Constraint for transmission line capacity [26]

$$-\bar{P}_{pq} \le \sum_{p \in \Omega_n} \left(\boldsymbol{G}_{l\text{-}p} P_{p,t}\right) - \sum_{q \in \Omega_n} \left(\boldsymbol{G}_{l\text{-}q} L_{q,t}\right) \le \bar{P}_{pq} \quad \forall p,q \in \Omega_n \tag{29}$$

where $P_{p,t}$ and $L_{q,t}$ are the generation and load demands at buses p and q, respectively; $\bar{P}_{pq}$ is the maximum power flow between buses p and q; $\boldsymbol{G}_{l\text{-}p}$ is the line-bus admittance matrix; and Ω_n is the set of buses.

8) Probability distribution set of random variables

Scenarios and probability distributions are obtained through scenario reduction from historical RG output samples. Based on the assumption that s typical scenarios are obtained after reduction, the probabilities p_s^0 can be expressed as [27]:

$$p_s^0 = \frac{N_s}{N} \quad \forall s \in S \tag{30}$$

where S is the set of typical scenarios; N is the total number of samples; and N_s is the number of original scenarios included in a typical scenario s. With p_s^0 used as the base probability density, the reference distribution is:

$$P^0 = \left\{ p_1^0, p_2^0, \dots, p_{|S|}^0 \right\} \tag{31}$$

Based on P^0, we construct Ω by considering the 1-norm and ∞-norm constraints [28]-[30]:

$$\Omega = \left\{ p_s \left| \begin{array}{l} p_s \ge 0, \forall s \in S \\ \sum\limits_{s \in S} p_s = 1 \\ \sum\limits_{s \in S} \left| p_s - p_s^0 \right| \le \dfrac{|S|}{2N} \ln \dfrac{2|S|}{1-\theta_1} \\ \max\limits_{s \in S} \left| p_s - p_s^0 \right| \le \dfrac{1}{2N} \ln \dfrac{2|S|}{1-\theta_\infty} \end{array} \right. \right\} \tag{32}$$

where p_s belongs to the set Ω, representing the probability of typical scenario s; and θ_1 and θ_∞ are the confidence levels at the 1-norm and ∞-norm, respectively.

B. Intraday Rescheduling Model

1) Objective Function

At the intraday stage, the objective function of rescheduling aims to minimize $C_t^{x,sub}$ and various penalty costs, which enhances ISO economic efficiency while ensuring a high level of operation reliability. The objective function is expressed as:

$$F_2 = \sum_{t \in T, x \in \{w,v,g,ess,tl\}} C_t^{x,sub} + \sum_{n \in N_V} C_{n,t}^{v,cur} + \sum_{m \in N_W} C_{m,t}^{w,cur} + \sum_{k \in N_L} C_{k,t}^{l,shed} \tag{33}$$

2) Constraints

The constraints for the intraday rescheduling model include upper-limit adjustment and post adjustment output constraints. Taking TGs as an example, we can obtain:

$$\Delta P_{i,t}^{g} \le \Delta \bar{P}_{i,t}^{g} \quad \forall i \in N_G, \forall t \in T \tag{34a}$$

$$u_{i,t}^{g} P_{i,t}^{g,b} \le P_{i,t}^{g} + \Delta P_{i,t}^{g} \le u_{i,t}^{g} \bar{P}_{i}^{g} \quad \forall i \in N_G, \forall t \in T \tag{34b}$$

$$\left(P_{i,t-1}^{g} + \Delta P_{i,t-1}^{g}\right) - \left(P_{i,t}^{g} + \Delta P_{i,t}^{g}\right) \le u_{i,t}^{g} R_i^{g,dn} - \left(u_{i,t}^{g} - u_{i,t-1}^{g}\right) P_{i,t}^{g,b} \quad \forall i \in N_G, \forall t \in T \tag{34c}$$

where $\Delta P_{i,t}^{g}$ is the output adjustment of TGs at the intraday stage. As cost allocation and compensation distribution occur intradaily, the constraints also include (8a) - (9b) and (14)-(21).

C. Solution

We divide the day-ahead DRO pre-scheduling model into a master problem (MP) and subproblem (SP) and solve them using the column-and-cut generation algorithm [31]. For the SP, the inner minimum problem is transformed into a set of equations with no objective under the Karush-Kuhn-Tucker conditions [32] and further incorporated into the outer maximization problem. The MP and SP are expressed as (35a) and (35b), respectively.

$$\begin{cases} \min_{\boldsymbol{x}} \left(\boldsymbol{c}^{\mathrm{T}} \boldsymbol{x} + a \right) \\ \text{s.t. } a \geq \sum_{s \in S} p_s \boldsymbol{d}^{\mathrm{T}} \boldsymbol{y} \\ \quad \boldsymbol{A}\boldsymbol{x} = \boldsymbol{i} \\ \quad \boldsymbol{C}\boldsymbol{x} \geq \boldsymbol{h} \\ \quad \boldsymbol{B}\boldsymbol{y} = \boldsymbol{l} \\ \quad \boldsymbol{K}\boldsymbol{y} \geq \boldsymbol{w} \\ \quad \boldsymbol{W}\boldsymbol{y} \geq \boldsymbol{N}\boldsymbol{\xi}_s \\ \quad \boldsymbol{F}\boldsymbol{x} + \boldsymbol{G}\boldsymbol{y} = \boldsymbol{g} \\ \quad \boldsymbol{J}\boldsymbol{x} + \boldsymbol{R}\boldsymbol{y} \geq \boldsymbol{r} \end{cases} \tag{35a}$$

$$\begin{cases} \max_{p_s \in \Omega, \boldsymbol{y} \in Y(\boldsymbol{x}, \boldsymbol{\xi}_s)} \sum_{s \in S} p_s \boldsymbol{d}^{\mathrm{T}} \boldsymbol{y} \\ \text{s.t. } \boldsymbol{B}\boldsymbol{y} = \boldsymbol{l} \\ \quad \boldsymbol{K}\boldsymbol{y} \geq \boldsymbol{w} \\ \quad \boldsymbol{W}\boldsymbol{y} \geq \boldsymbol{N}\boldsymbol{\xi}_s \\ \quad \boldsymbol{F}\boldsymbol{x} + \boldsymbol{G}\boldsymbol{y} = \boldsymbol{g} \\ \quad \boldsymbol{J}\boldsymbol{x} + \boldsymbol{R}\boldsymbol{y} \geq \boldsymbol{r} \\ \quad \boldsymbol{0} \leq \boldsymbol{\pi}_1 \perp \left(\boldsymbol{w} - \boldsymbol{K}\boldsymbol{y} \right) = \boldsymbol{0} \\ \quad \boldsymbol{0} \leq \boldsymbol{\pi}_2 \perp \left(\boldsymbol{N}\boldsymbol{\xi}_s - \boldsymbol{W}\boldsymbol{y} \right) = \boldsymbol{0} \\ \quad \boldsymbol{0} \leq \boldsymbol{\pi}_3 \perp \left(\boldsymbol{r} - \boldsymbol{J}\boldsymbol{x} - \boldsymbol{R}\boldsymbol{y} \right) = \boldsymbol{0} \\ \quad \nabla_y L\left(\boldsymbol{y}, \boldsymbol{\pi}_{1\text{-}5} \right) = \boldsymbol{0} \end{cases} \tag{35b}$$

where a is the auxiliary variable representing an upper bound on the objective value of the SP; $\boldsymbol{c}$ and $\boldsymbol{d}$ are the column vectors of coefficients in (22a); $\boldsymbol{A}$, $\boldsymbol{B}$, $\boldsymbol{C}$, $\boldsymbol{F}$, $\boldsymbol{G}$, $\boldsymbol{J}$, $\boldsymbol{K}$, $\boldsymbol{N}$, $\boldsymbol{R}$, and $\boldsymbol{W}$ are the coefficient matrices of variables under their corresponding constraints; $\boldsymbol{g}$, $\boldsymbol{h}$, $\boldsymbol{i}$, $\boldsymbol{l}$, $\boldsymbol{r}$, and $\boldsymbol{w}$ are the constant column vectors; $\boldsymbol{\xi}_s$ is the RG output in typical scenario s; $L(\cdot)$ is the Lagrange function; $Y(\cdot)$ is the feasible region given $\boldsymbol{x}$ and $\boldsymbol{\xi}_s$; and $\boldsymbol{\pi}_1$-$\boldsymbol{\pi}_3$ and $\boldsymbol{\pi}_{1\text{-}5}$ are the Lagrange multipliers introduced for inequality and equality constraints, respectively. The specific linearization methods and solution flow can be found in [33].

As Fig. 3 shows, at the day-ahead stage, the ISO solves the DRO pre-scheduling model, whereas the binary variables corresponding to TGs, ESSs, and TLs participating in the peak regulation are fixed at the intraday stage. The outputs of the nonpeak regulation TGs and ESSs are also fixed at the intraday stage. In addition, the prescheduled results for all peak regulation participants are transferred to the intraday stage for reference purposes. At the intraday stage, the rescheduling model is solved through rolling optimization [34], and the proposed mechanism is implemented.

V. Case Study

In this section, we present numerous case studies demonstrating the effectiveness of the proposed mechanism and day-ahead DRO pre-scheduling model. These experiments are performed using Gurobi 10.0.0 using MATLAB R2022a on a personal computer with an AMD Core (Ryzen 9 6900HX) and 16 GB of memory.

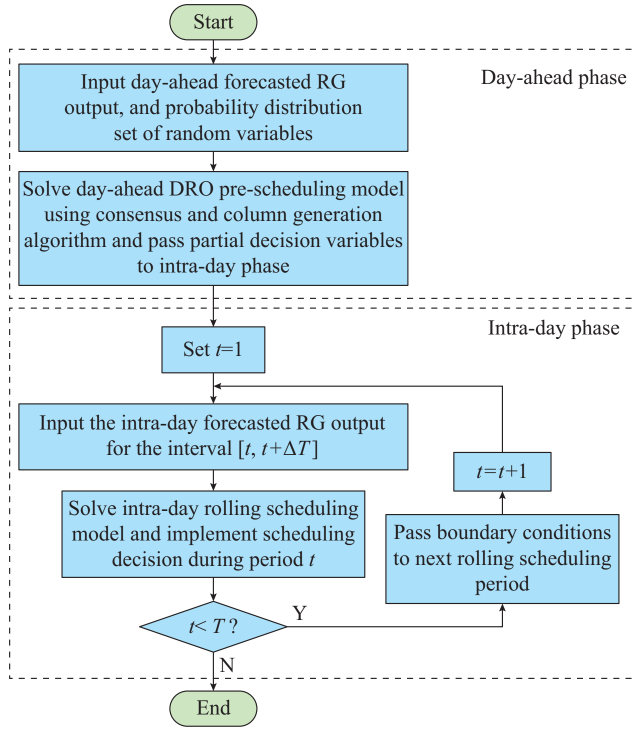

Fig. 3. Flowchart for proposed day-ahead DRO pre-scheduling model.

The basic data for the IEEE 30-bus system can be obtained from [35]. The IEEE 30-bus system includes 6 TGs with units 2, 4, and 6 participating in the proposed mechanism. The ESS has a charging/discharging power limit of 100 MW and a capacity limit of 300 MWh, with an initial SOC of 0.5. Table I lists the operation parameters of TG and Table II presents the node information and participation status of all PRRs.

TABLE I
Operation Parameters of TG

Unit	$\overline{P}_i^{g}$ (MW)	$\overline{P}_i^{g,rpr}$ (MW)	$\underline{P}_i^{g,rpr}$ (MW)	$P_i^{g,a}$ (MW)	$P_i^{g,b}$ (MW)
1	500	420	250	180	80
2	350	300	180	120	60
3	120	100	60	40	30
4	120	100	60	40	30
5	150	120	80	60	40
6	150	120	80	60	40

TABLE II
Node Information and Participation Statuses of All PRRs

Resource	Node	Participation status
ESS	24	√
PV	8	√
WT	20	√
TL1	24, 25, 26, 27, 28, 29, 30	√
TL2	12, 13, 14, 15, 18, 23	
TL3	1, 2, 3, 4, 5, 6, 7, 8	√
TL4	9, 10, 11, 16, 17, 19, 20, 21, 22	

A. Construction Effectiveness Analysis of Peak Regulation-friendly Output Curves

We next validate the construction effectiveness of peak regulation-friendly output curves. The values of v_x, a^g, a^{ess}, and a^{tl} are set to be 0.2, 0.01, 100, and 10, respectively. Figure 4 presents the peak regulation-friendly output curves and forecasted output curves.

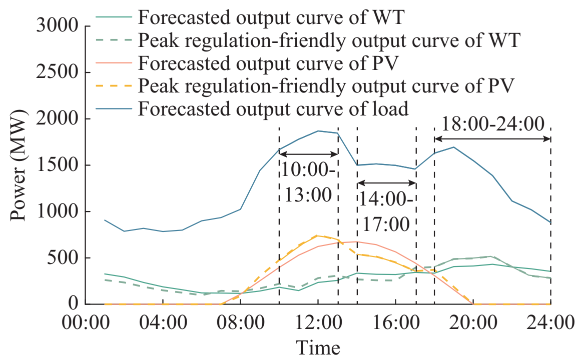

Fig. 4. Peak regulation-friendly output curve and forecasted output curve.

As Fig. 4 shows, the peak regulation-friendly output of PV is higher than the forecasted output from 10:00 to 13:00 and lower than the forecasted output of PV from 14:00 to 17:00, aligning with the trend of the mid-day peak load. Similarly, the peak regulation-friendly output curve of WT aligns with the evening peak load trend from 18:00 to 24:00. Therefore, the peak regulation-friendly output curve exhibits higher similarity than the load curve.

Furthermore, we use peak regulation-friendly output curves and forecasted output curves as inputs to solve the general economic scheduling model [36] and calculate f^g, f^{ess}, and f^{tl}. The calculation methods are expressed in (10b)-(10d).

Table III shows that using the peak regulation-friendly output curves as inputs results in a decrease in f^g, f^{ess}, and f^{tl}. f^{tl} shows the greatest decrease due to the high compatibility of the peak regulation-friendly output curves with the load curve. The previous analysis further demonstrates the construction effectiveness of the peak regulation-friendly output curve.

TABLE III
COMPARISON OF INDICATORS FOR PEAK REGULATION PRESSURE

RG output	f^g	f^{ess}	f^{tl}
Forecasted output	262864.12	0.55	267.96
Peak regulation-friendly output	180190.57	0.02	0

B. Effectiveness Analysis of Proposed Mechanism

Since the proposed mechanism considers the satisfaction of PRRs and the waveform difference of RGs as key parameters, we design multiple cases for the analysis in this section. Case 1 applies the proposed mechanism. Case 2 does not consider the satisfaction of PRRs. Case 3 does not consider the waveform difference of RG. In Case 2, because the satisfaction of PRRs is not considered, the ISO does not subsidize them, and they receive compensation based solely on their contributions. In Case 3, because the waveform differences are not considered, the allocation ratios are related only to the proportion of RG outputs.

For Cases 1 and 2, we introduce the compensation-to-cost ratio (CCR) (which includes ISO subsidy in Case 1) as an evaluation indicator. CCRs in Cases 1 and 2 are calculated as:

$$CCR = \frac{C_t^{x,comp} + C_t^{x,sub}}{C_t^{x,pr}} \quad \forall t, x \in \{g, ess, tl\} \tag{36a}$$

$$CCR = \frac{C_t^{x,comp}}{C_t^{x,pr}} \quad \forall t, x \in \{g, ess, tl\} \tag{36b}$$

Table IV clearly shows that no CCR in Case 1 falls below 1, which demonstrates that the proposed mechanism considering satisfaction ensures that each PRR receives compensation exceeding its peak regulation costs, thus securing financial benefits. In addition, in Case 1, the ISO subsidy for TGs is significantly higher than that for the other PRRs. This is because the cost of TGs to participate in peak regulation is higher than that of the ESSs and TLs. If the satisfaction of PRRs is not considered, TGs would only earn compensation based on their peak regulation contributions, which would result in significant losses for their earnings. The previous analysis demonstrates that the proposed mechanism not only ensures the benefits of all PRRs but is also more favorable for resources with higher peak regulation costs, thus aiding its implementation in practical engineering projects.

TABLE IV
COMPARISON RESULTS OF CASES 1 AND 2

Component	Case 1			Case 2	
	CCR	Compensation cost ($)	ISO subsidy ($)	CCR	Compensation cost ($)
TG2	1.25	226.82	331.66	0.67	1302.72
TG4	1.26	3702.93	1500.92	0.74	2965.24
TG6	1.26	6192.17	2741.49	0.86	6139.22
TL1	1.59	444.17	62.03	1.57	616.01
TL3	1.37	1945.74	357.70	1.38	3244.70
ESS	2.71	2001.27	246.99	5.57	1924.67

Figures 5 and 6 illustrate the peak regulation cost allocation in Cases 1 and 3, respectively, and the time interval is 15 min. The largest difference is observed between 13:00 and 18:00. During these periods, both the WT and PV have high power outputs, leading to a high allocation ratio for the WT and PV in Case 3. By contrast, Case 1 adjusts the allocation ratio based on the waveform difference, which accounts for the friendliness of the output.

Figure 7 illustrates the allocation ratio variation trend among the RGs in Case 1, along with the peak regulation-friendly output curves and forecasted outputs. The figure clearly shows that, although the forecasted output of the PV system is higher at 13:00 than that at 12:00, its allocation ratio is lower because the forecasted output at 13:00 closely matches the peak regulation-friendly output curve.

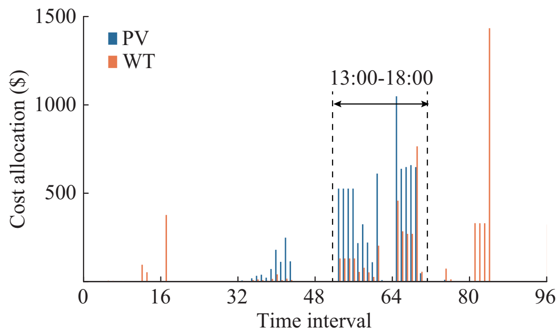

Fig. 5. Peak regulation cost allocation in Case 1.

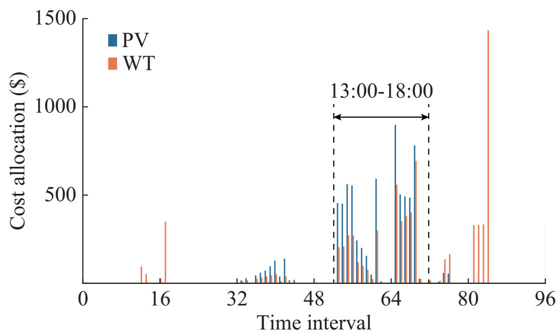

Fig. 6. Peak regulation cost allocation in Case 3.

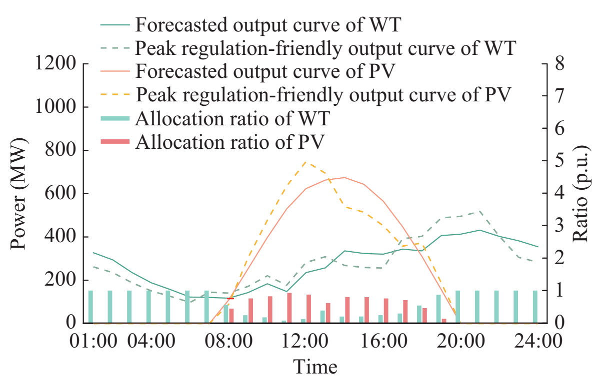

Fig. 7. Allocation ratio variation trend among RGs and power in Case 1.

In addition, the allocation ratio of PV at 08:00 and 09:00 reveals that, although the respective waveform differences of RGs are nearly constant, the allocation ratio of PV at 09:00 is higher than that at 08:00 due to a significant increase in the forecasted output of PV as compared with that of WT.

The previous analysis demonstrates that when using the proposed mechanism for peak regulation cost allocation, it not only considers the RG output but also incorporates the waveform difference between the peak regulation-friendly output curves and the forecasted output curves, thus considering the friendliness of RGs from a system perspective. Compared with the mechanism based solely on power output, the proposed mechanism is more reasonable.

To further validate the effectiveness of the proposed mechanism in cases with increasing RG output, we construct multiple cases in this subsection. Case 1 considers that all data remain the same. Cases 2-5 consider that the forecasted RG output during each time period increases sequentially by 1.05, 1.10, 1.15, and 1.20 times, forming new forecasted output curves.

In addition, we introduce two evaluation indicators: subsidy-to-cost ratio (SCR) and RG net allocation-to-revenue ratio (RGNARR). The calculation methods for them are expressed as:

$$SCR = \frac{\sum\limits_{t\in T, x\in\{g,ess,tl,w,v\}} C_t^{x,sub}}{\sum\limits_{t\in T} C_t^{pr}} \tag{37}$$

$$RGNARR = \frac{\sum\limits_{t\in T, x\in\{w,v\}} \left(C_t^{x,alloc} - C_t^{x,sub}\right)}{p^e\left(P_t^x - P_t^{x,cur}\right)} \tag{38}$$

The indicator results for various cases are presented in Table V. As the RG outputs increase, both the peak regulation cost and the ISO subsidy increase. According to the proposed mechanism, ISO is required to provide subsidies to both RGs and PRRs, which leads to a greater increase in ISO subsidy compared with the increase in peak regulation cost. As a result, the SCR also increases. Nevertheless, the maximum SCR value remains at only 59.85% across all cases, indicating that the proposed mechanism effectively allocates and distributes the peak regulation cost and compensation among the RGs and PRRs. This significantly reduces the traditional policy-driven peak regulation subsidy for the PRRs paid by the ISO.

TABLE V
INDICATOR RESULTS FOR VARIOUS CASES

Case	SCR (%)	RGNARR (%)
1	46.36	3.62
2	49.90	2.49
3	53.21	2.91
4	56.12	3.31
5	59.85	3.12

In addition, the RGNARR remains low across all cases, indicating that after the subsidy provided by the ISO to the RGs is considered, the net allocation cost provided by the RGs is significantly lower than their revenue from power generation, ensuring the interests of the RGs.

C. Economic Analysis of Scheduling Model When Proposed Mechanism is Applied

We next analyze the economic impact of the proposed mechanism on power system scheduling. This section includes two cases. Case 1 applies the proposed mechanism. Case 2 applies the regular economic scheduling model, with ISO bearing all peak regulation costs (ISO subsidy equals cost).

Table VI shows that the proposed mechanism significantly reduces the ISO subsidy by effectively allocating the peak regulation cost generated by the PRRs among the RGs, thereby cutting ISO subsidy expenditures and enhancing the operation economy. In addition, the zero-penalty cost indicates that the proposed mechanism ensures operation reliability.

TABLE VI
COMPARISON OF COSTS BETWEEN TWO CASES

Case	Total cost ($)	ISO subsidy ($)	Peak regulation cost ($)	Penalty cost ($)
1	691669.59	5240.79	14513.18	0
2	697786.00	16204.06	16204.06	0

Figure 8 shows the variation trends of the ISO subsidy for the PRRs in Cases 1 and 2, and the time interval is 15 min.

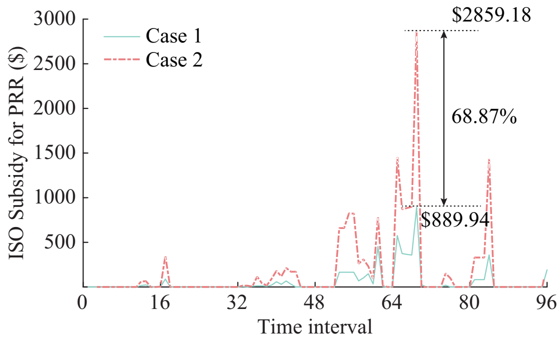

Fig. 8. Variation trends of ISO subsidy for PRR in Cases 1 and 2.

The variation trend is similar for the two cases, with the ISO subsidy peaking in the afternoon, which aligns with periods of high RG generation. Therefore, significant adjustments in PRR outputs are necessitated to ensure complete renewable energy absorption, generating high peak regulation costs during these periods. Although the overall trends of the two curves exhibit similarity, the difference in their magnitudes is notable, with the maximum discrepancy reaching $1969.24, which is translated to a substantial reduction of 68.87%. This analysis shows that the proposed mechanism can reduce policy-driven subsidies in regular economic scheduling, particularly when high levels of RGs are generated.

To further analyze the differences in resource scheduling between the two cases, Table VII presents the electricity of the peak regulation and associated cost for each PRR.

TABLE VII
ELECTRICITY OF PEAK REGULATION AND ASSOCIATED COST FOR EACH PRR

Component	Case 1		Case 2	
	Electricity (MWh)	Cost ($)	Electricity (MWh)	Cost ($)
TG2	2.08	444.18	8.80	1941.73
TG4	23.71	4138.70	22.70	4008.01
TG6	42.00	7105.05	42.00	7171.33
TL1	10.68	318.48	13.05	392.92
TL3	56.19	1675.66	77.90	2344.86
ESS	30.44	831.11	21.47	345.21
Total	165.09	14513.18	185.92	16204.06

Table VII shows that the pre-scheduling model that considers the proposed mechanism reduces the total electricity of the peak regulation and associated costs. This is because, after considering the proposed mechanism, the ISO balances the relationship between the peak regulation electricity and the compensation/subsidy received by PRRs during the intraday adjustment. This ensures that the resource scheduling results maximally satisfy the self-balance between the peak regulation cost/compensation among the PRRs and RGs, thereby enhancing the economic efficiency of the system.

D. Comparative Analysis of Various Mechanisms

To demonstrate the superiority of the proposed mechanism, we present a comparative analysis with the similar mechanism in [37]. Reference [37] calculates the peak regulation compensation of PRRs based on the peak regulation of electricity and the unit compensation price, improving the existing mechanism of peak regulation cost allocation and compensation distribution. Recipients of peak regulation services are allowed to bear the compensation costs. Notably, in [37], TGs without providing peak regulation services are still required to bear the peak regulation costs. For consistency, we uniformly exclude these TGs from the cost allocation in the case study. Further details can be found in [37].

The comparison of compensation distributions between two mechanisms are shown in Fig. 9. The figure shows that within the same category of PRRs, the peak regulation electricity and the corresponding compensation are generally proportional, which demonstrates the fairness of the proposed mechanism. However, the compensation is significantly lower when the mechanism in [37] is used. The unit compensation price in [37] is determined through market clearing, which may lead to PRRs receiving either insufficient or excessive compensation [37]. By contrast, we treat peak regulation costs as total compensation and include a small ISO subsidy to ensure that all the compensation that the PRRs receive exceeds their costs. The proposed mechanism ensures that PRRs are motivated to participate in peak regulation and prevents both under- and over-compensation.

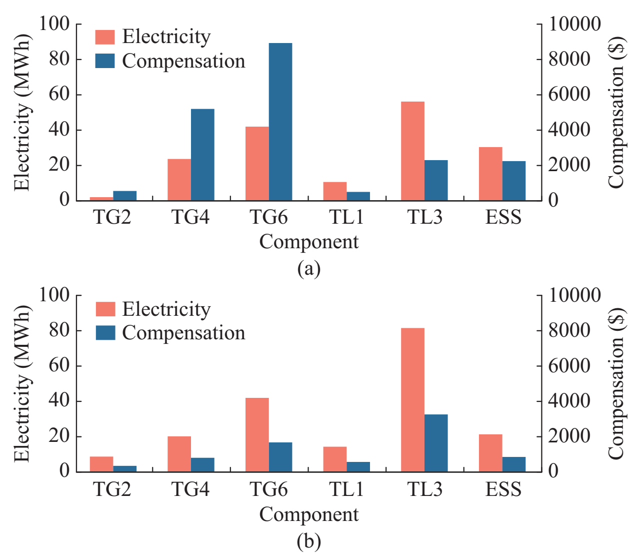

Fig. 9. Comparison of compensation distributions between two mechanisms. (a) Proposed mechanism. (b) Mechanism in [37].

Besides, we compare the variation trends in the allocation ratios for peak regulation costs or compensation. Figure 10 shows that some differences exist in the allocation ratios between the two mechanisms. We further analyze the forecasted power of WT, PV, and load during certain periods, as shown in Fig. 11. At 13:00, both the load and PV power are close to their daily peaks, with the PV providing significant power support, which is beneficial for system operation. Therefore, the PV ratio under the proposed mechanism is lower. However, at 14:00, the load starts to decline, whereas the PV power continues to increase slightly, which introduces certain risk to the system operation. As a result, the PV ratio at 14:00 under the proposed mechanism is higher than that under the mechanism in [37]. In short, the proposed mechanism considers the friendliness of RGs when the allocation ratio is determined. Compared with other mechanisms that determine only the allocation ratio based on the generation power, the proposed mechanism is more reasonable.

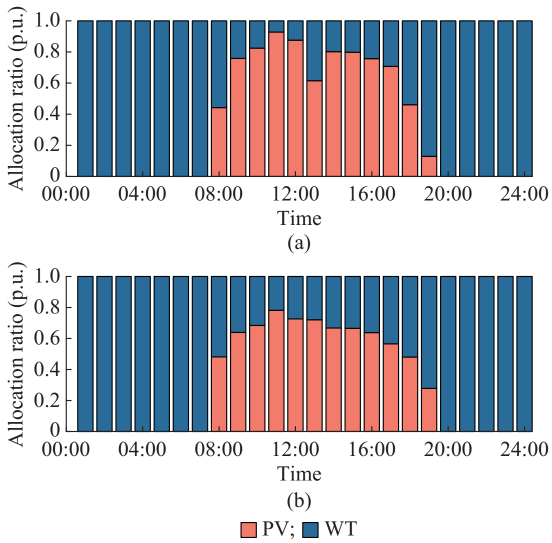

Fig. 10. Comparison of allocation ratios between two mechanisms. (a) Proposed mechanism. (b) Mechanism in [37].

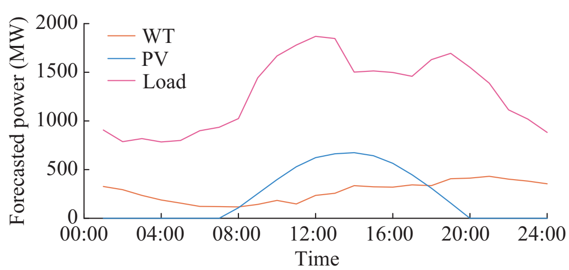

Fig. 11. Forecasted power of WT, PV, and load.

VI. Conclusion

We design a mechanism for peak regulation cost allocation and compensation distribution that considers participant satisfaction and in turn constructs a coordinated generation scheduling model. The conclusions are as follows.

1) The peak regulation-friendly output curves significantly lower the peak regulation pressure as compared with the forecasted RG outputs, providing a basis for assessing the allocation ratios among various RGs.

2) The proposed mechanism effectively allocates peak regulation costs and distributes compensation, thus favoring PRRs with higher peak regulation costs. In addition, the proposed mechanism is well-suited for future power system operation scenarios with high volumes of renewable energy. A comparative analysis shows that the proposed mechanism not only avoids insufficient or excessive compensation but also offers a more reasonable method for determining the allocation ratios for RGs.

3) The coordinated generation scheduling model based on the proposed mechanism significantly reduces the ISO subsidy while ensuring load supply security and renewable energy accommodation. The model can also reduce both electricity consumption during peak regulation and the associated costs through coordinated generation scheduling among various resources, further enhancing economic efficiency.

The forecasted RG output is reported by the RG operators, and we do not specifically account for the possibility of RG operators submitting unreliable data at the day-ahead stage when designing the proposed mechanism. The reliability of the data submitted by the RGs significantly affects the fairness of the operation of the proposed mechanism. In future research, we will adopt a more comprehensive method for designing similar mechanisms. For example, we may introduce a data reliability assessment mechanism or adjust the allocation ratios during the intraday rolling stage based on the actual generation of the RGs to eliminate the negative effects of unreliable data submitted at the day-ahead stage. In addition, with the emergence of ISOs, the connection between power system dispatch and market clearing has become increasingly important. Designing optimization scheduling methods or allocation-distribution mechanisms without considering the electricity market may lead to issues such as mismatches between dispatch results and market clearing. Our future work will adopt a more comprehensive method to ensure that our results align better with practical engineering applications.

References

[1] E. E. El-Araby and N. Yorino, "A demand side response scheme for enhancing power system security in the presence of wind power," *International Journal of Electrical Power & Energy Systems*, vol. 146, p. 108714, Mar. 2023.

[2] S. Wang, F. Li, G. Zhang *et al.*, "Analysis of energy storage demand for peak shaving and frequency regulation of power systems with high penetration of renewable energy," *Energy*, vol. 267, p. 126586, Mar. 2023.

[3] X. Geng, Y. Zhou, W. Zhao *et al.*, "Pricing ancillary service of a Francis hydroelectric generating system to promote renewable energy integration in a clean energy base: tariff compensation of deep peak regulation," *Renewable Energy*, vol. 226, p. 120292, May 2024.

[4] Y. Chen, X. Feng, Z. Li *et al.*, "Multi-stage coordinated operation of a multi-energy microgrid with residential demand response under diverse uncertainties," *Energy Conversion and Economics*, vol. 1, no. 1, pp. 20-33, Sept. 2020.

[5] W. Zhu, X. Xu, B. Ding *et al.*, "Cooperative game-based energy storage planning for wind power cluster aggregation station," *Energy Reports*, vol. 11, pp. 4021-4031, Jun. 2024.

[6] J. Dong, G. Xue, R. Li *et al.*, "Research on peak shaving costs and allocation of wind power integration using scalable computing method," *Cluster Computing*, vol. 20, no. 1, pp. 391-400, Jan 2017.

[7] W. Wu, J. Zhu, Y. Chen *et al.*, "Modified shapley value-based profit allocation method for wind power accommodation and deep peak regu-

lation of thermal power," *IEEE Transactions on Industry Applications*, vol. 59, no. 1, pp. 276-288, Jan. 2023.

[8] Y. Wang, L. Yang, J. Li *et al*., "Quantitative and apportionment method of auxiliary service cost of new energy subject," in *Proceedings of 2023 2nd International Conference on Smart Grids and Energy Systems (SGES)*, Guangzhou, China, Aug. 2023, pp. 357-363.

[9] Y. Zhang, Y. Li, and G. Zhang, "Short-term wind power forecasting approach based on Seq2Seq model using NWP data," *Energy*, vol. 213, p. 118371, Dec. 2020.

[10] J. Zhu, Y. Miao, H. Dong *et al*., "Short-term residential load forecasting based on *k*-shape clustering and domain adversarial transfer network," *Journal of Modern Power Systems and Clean Energy*, vol. 12, no. 4, pp. 1239-1249, Jul. 2024.

[11] H. Jahangir, S. S. Gougheri, B. Vatandoust *et al*., "Plug-in electric vehicle behavior modeling in energy market: a novel deep learning-based approach with clustering technique," *IEEE Transactions on Smart Grid*, vol. 11, no. 6, pp. 4738-4748, Nov. 2020.

[12] B. Yang, X. Cao, Z. Cai *et al*., "Unit commitment comprehensive optimal model considering the cost of wind power curtailment and deep peak regulation of thermal unit," *IEEE Access*, vol. 8, pp. 71318-71325, Mar. 2020.

[13] Y. Zhao, C. Wang, Z. Zhang *et al*., "Flexibility evaluation method of power system considering the impact of multi-energy coupling," *IEEE Transactions on Industry Applications*, vol. 57, no. 6, pp. 5687-5697, Nov. 2021.

[14] W. Lin, Z. Yang, and J. Yu, "Flexibility of interconnected power system operation: analysis, evaluation and prospection," *Energy Conversion and Economics*, vol. 1, no. 3, pp. 141-150, Dec. 2020.

[15] M. Lu, J. Guan, H. Wu *et al*., "Day-ahead optimal dispatching of multi-source power system," *Renewable Energy*, vol. 183, pp. 435-446, Jan. 2022.

[16] X. Li, W. Li, R. Zhang *et al*., "Collaborative scheduling and flexibility assessment of integrated electricity and district heating systems utilizing thermal inertia of district heating network and aggregated buildings," *Applied Energy*, vol. 258, p. 114021, Jan. 2020.

[17] Q. Liu, J. Zhao, Y. Shao *et al*., "Multi-power joint peak-shaving optimization for power system considering coordinated dispatching of nuclear power and wind power," *Sustainability*, vol. 11, no. 17, p. 4801, Sept. 2019.

[18] B. Zhou, D. Xu, C. Li *et al*., "Optimal scheduling of biogas-solar-wind renewable portfolio for multicarrier energy supplies," *IEEE Transactions on Power Systems*, vol. 33, no. 6, pp. 6229-6239, Nov. 2018.

[19] M. Z. Oskouei, H. Mehrjerdi, D. Babazadeh *et al*., "Resilience-oriented operation of power systems: hierarchical partitioning-based approach," *Applied Energy*, vol. 312, p. 118721, Apr. 2022.

[20] L. Wang, W. Wu, Q. Lu *et al*., "Optimal aggregation approach for virtual power plant considering network reconfiguration," *Journal of Modern Power Systems and Clean Energy*, vol. 9, no. 3, pp. 495-501, May 2021.

[21] M. Guerrero, F. G. Montoya, R. Baños *et al*., "Community detection in national-scale high voltage transmission networks using genetic algorithms," *Advanced Engineering Informatics*, vol. 38, pp. 232-241, Oct. 2018.

[22] H. Hou, M. Xue, Y. Xu *et al*., "Multi-objective economic dispatch of a microgrid considering electric vehicle and transferable load," *Applied Energy*, vol. 262, p. 114489, Mar. 2020.

[23] X. Zhao, D. Ru, P. Wang *et al*., "Fatigue life prediction of a supercritical steam turbine rotor based on neural networks," *Engineering Failure Analysis*, vol. 127, p. 105435, Sept. 2021.

[24] Y. Meng, S. Fan, Y. Shen *et al*., "Transmission and distribution network-constrained large-scale demand response based on locational customer directrix load for accommodating renewable energy," *Applied Energy*, vol. 350, p. 121681, Nov. 2023.

[25] A. M. Youssef, T. K. Abdel-Galil, E. F. El-Saadany *et al*., "Disturbance classification utilizing dynamic time warping classifier," *IEEE Transactions on Power Delivery*, vol. 19, no. 1, pp. 272-278, Jan. 2004.

[26] C. Shao, X. Wang, M. Shahidehpour *et al*., "Power system economic dispatch considering steady-state secure region for wind power," *IEEE Transactions on Sustainable Energy*, vol. 8, no. 1, pp. 268-278, Jan. 2017.

[27] Y. Chen, Q. Guo, H. Sun *et al*., "A distributionally robust optimization model for unit commitment based on Kullback-Leibler divergence," *IEEE Transactions on Power Systems*, vol. 33, no. 5, pp. 5147-5160, Sept. 2018.

[28] F. Alismail, P. Xiong, and C. Singh, "Optimal wind farm allocation in multi-area power systems using distributionally robust optimization approach," *IEEE Transactions on Power Systems*, vol. 33, no. 1, pp. 536-544, Jan. 2018.

[29] P. Li, L. Song, J. Qu *et al*., "A two-stage distributionally robust optimization model for wind farms and storage units jointly operated power systems," *IEEE Access*, vol. 9, pp. 111132-111142, Jul. 2021.

[30] S. He, H. Gao, Z. Chen *et al*., "Data-driven worst conditional value at risk energy management model of energy station," *Energy*, vol. 266, p. 126421, Mar. 2023.

[31] H. Huang, M. Zhou, S. Zhang *et al*., "Exploiting the operational flexibility of wind integrated hybrid AC/DC power systems," *IEEE Transactions on Power Systems*, vol. 36, no. 1, pp. 818-826, Jan. 2021.

[32] O. Homaee, A. Najafi, M. Jasinski *et al*., "Coordination of neighboring active distribution networks under electricity price uncertainty using distributed robust bi-level programming," *IEEE Transactions on Sustainable Energy*, vol. 14, no. 1, pp. 325-338, Jan. 2023.

[33] B. Zeng and L. Zhao, "Solving two-stage robust optimization problems using a column-and-constraint generation method," *Operations Research Letters*, vol. 41, no. 5, pp. 457-461, Sept. 2013.

[34] D. Feng, F. Wu, Y. Zhou *et al*., "Multi-agent-based rolling optimization method for restoration scheduling of distribution systems with distributed generation," *Journal of Modern Power Systems and Clean Energy*, vol. 8, no. 4, pp. 737-749, Jul. 2020.

[35] IEEE. (2008, Jun.). IEEE 30-bus system. [Online]. Available: https://labs.ece.uw.edu/p stca/pf30/ieee30cdf.txt

[36] N. Yan, Z. Xing, W. Li *et al*., "Economic dispatch application of power system with energy storage systems," *IEEE Transactions on Applied Superconductivity*, vol. 26, no. 7, pp. 1-5, Oct. 2016.

[37] Y. Wang, Y. Wang, C. Liu *et al*., "Auxiliary service dynamic compensation mechanism design for incentivizing market participants to provide flexibility in China," *Protection and Control of Modern Power Systems*, vol. 9, no. 5, pp. 112-128, Sept. 2024.

Yida Yang received the B.E. degree in electrical engineering from the China University of Petroleum (East China), Qingdao, China, in 2023. He is currently pursuing the M.Sc. degree in electrical engineering in Sichuan University, Chengdu, China. His research interests include power system scheduling optimization and peak regulation optimization.

Hongjun Gao received the B.S., M.S., and Ph.D. degrees in electrical engineering from Sichuan University, Chengdu, China, in 2011, 2014, and 2017, respectively. From 2015 to 2016, he was a Visiting Scholar with the Department of Electrical Engineering and Computer Science, University of Wisconsin-Milwaukee, Milwaukee, USA. He is currently an Associate Professor with the College of Electrical Engineering, Sichuan University. His research interests include planning and operation of active distribution system, economic dispatch, distributed generation integration, and multi-energy system optimization.

Yingmeng Xiang received the Ph.D. degree in electrical engineering from the University of Wisconsin-Milwaukee, Milwaukee, USA, in 2018. His research interests include Internet of Things for power system, artificial intelligence, smart grid reliability, and cyber-physical system resilience.

Minghao Guo received the B.S. and M.S. degrees from Changchun University of Technology, Changchun, China, in 2020 and 2023. He is currently pursuing the Ph.D. degree in Sichuan University, Chengdu, China. His research interests include power system balance analysis and distributed optimal scheduling.

Jiye Wang is currently a Ph.D. Supervisor and a Senior Engineer with China Electric Power Research Institute, Beijing, China. His research interests include Energy Internet and smart grid.

Junyong Liu received the Ph.D. degree in electrical engineering from Brunel University, Uxbridge, U.K., in 1998. He is currently a Professor with the College of Electrical Engineering, Sichuan University, Chengdu, China. He is the Director of the Sichuan Province Key Smart Grid Laboratory, Chengdu, China. His research interests include power system planning, operation, electricity market, artificial intelligence, and computer application.